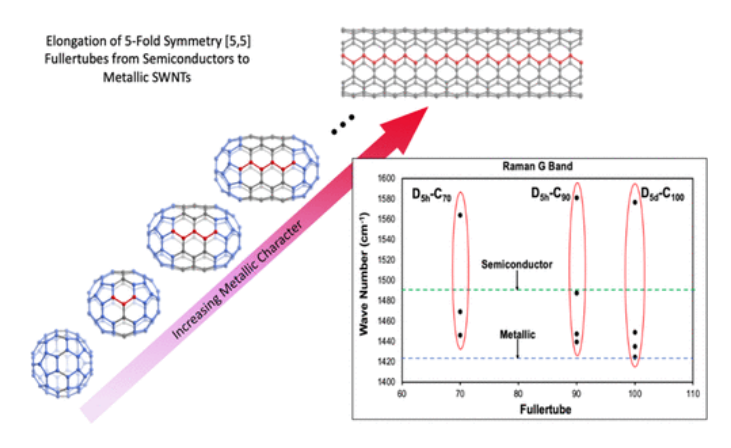
# Semiconducting and Metallic [5,5] Fullertube Nanowires: Characterization of Pristine $D_{5h}(1)$ - $C_{90}$ and $D_{5d}(1)$ - $C_{100}$

Steven Stevenson\*, Xiaoyang Liu, D. Mathew Sublett Jr., Ryan M. Koenig, Tiffany L. Seeler, Katelyn R. Tepper, Hannah M. Franklin, Xiaoling Wang, Rong Huang, Xu Feng, Kevin Cover, Diego Troya, Narasimhamurthy Shanaiah, Robert J. Bodnar, and Harry C. Dorn\*

### **Abstract**

Although fullerenes were discovered nearly 35 years ago, scientists still struggle to isolate "single molecule" tubular fullerenes larger than  $C_{90}$ . In similar fashion, there is a paucity of reports for pristine single-walled carbon nanotubes (SWNTs). In spite of Herculean efforts, the isolation and properties of pristine members of these carbonaceous classes remain largely unfulfilled. For example, the low abundance of spherical and tubular higher fullerenes in electric-arc extracts (<0.01–0.5%) and multiplicity of structural isomers remain a major challenge. Recently, a new isolation protocol for highly tubular *fullerenes*, also called fullertubes, was reported. Herein, we describe spectroscopic characterization including  $^{13}$ C NMR, XPS, and Raman results for purified [5,5] fullertube family members,  $D_{5h}$ - $C_{90}$  and  $D_{5d}$ - $C_{100}$ . In addition, DFT computational HOMO–LUMO gaps, polarizability indices, and electron density maps were also obtained. The Raman and  $^{13}$ C NMR results are consistent with semiconducting and metallic properties for  $D_{5h}$ - $C_{90}$  and  $D_{5d}$ - $C_{100}$ , respectively. Our report suggests that short [5,5] fullertubes with aspect ratios of only  $\sim$ 1.5–2 are metallic and could exhibit unique electronic properties.



## Introduction

Publications are ubiquitous for  $C_{60}$  and  $C_{70}$  fullerenes; yet only a few studies exist for pristine samples of higher fullerenes (e.g.,  $C_{90}$  and higher). Reasons for this paucity of reports include: (1) typical yields less than 0.5%, (2) low solvent solubility, (3) inefficient separation methods, and (4) occurrence of only trace amounts of pristine and isomerically pure samples. Because the number of possible structural isomers increases with cage size, the complexity of fullerene extracts increases as well. While,  $I_h$ - $C_{60}$  and  $D_{5h}$ -

 $C_{70}$  each have one structural isomer that obeys the isolated pentagon (IPR) rule, there are 46 and 450 candidate IPR structural isomers for  $C_{90}$  and  $C_{100}$ , respectively. (1) If only HPLC is used for separation, the co-elution of fullerenes and their structural isomers is often a very difficult obstacle to overcome. For example, multiple isomers of  $C_{90}$  have been chromatographically isolated (2–5) and their structures have been determined by X-ray crystallography. (3–5) The similarity of retention times among various  $C_{90}$  isomers on various HPLC columns is problematic. In the work of Xu et al., (2) three unique stationary phases were needed. Their initial fullerene and metallofullerenes mixture first used a PYE column, then a Buckyprep column, and finally a Buckyprep-M column to resolve and isolate  $C_{90}$  isomers I and II. Subsequently, three structural isomers of  $C_{90}$  were isolated using a three-stage HPLC process of Buckyprep-M, Buckyprep, and PBB columns by Yang et al. (3,4) Their crystallographic analysis provided purified  $C_{90}$  samples of  $C_{1}(30)$ - $C_{90}$ ,  $C_{1}(32)$ - $C_{90}$ , and the  $D_{5h}(1)$ - $C_{90}$  tubular isomer. (3–5) Further, the process of growing suitable crystals for X-ray structural analysis can be a time process.

Simultaneous to the progress toward obtaining pristine higher fullerenes, a similar goal but different approach has been explored in carbon nanotube (CNT) chemistry. Since the independent discovery of single-walled carbon nanotubes (SWNTs) by lijima and Bethune in 1991, a (n,m) indices descriptor has been employed to describe the length and circular vector for the hexagon sheet before roll-up as a singlewall carbon nanotube (SWNT).(6,7) Specifically, most zigzag SWNTs (n > 0, m = 0) are semiconducting, but armchair SWNTs (n = m) are expected to exhibit metallic behavior. In 1992, DFT studies by Mintmire and colleagues reported that a [5,5] nanotube would have room temperature metallic character and carrier mobility along the tubular axis comparable to metals. (8) Moreover, in contrast with normal metallic wires, it is reported that armchair nanotubes exhibit an effective disorder that increases with the CNT's diameter and should result in exceptional ballistic transport properties for large diameter (n = m) CNTs.(9) The methods for generating CNTs from graphite invariably produce mixtures of zigzag and armchair tubes of varying chirality, diameters and lengths. Hence, their separation has proven to be virtually impossible on a practical scale. An alternative strategy is an organic synthesis approach that employs an end-cap template or short CNT that can be elongated by successive annulated ring growth toward longer CNTs. Scott and co-workers have elegantly described the preparation of a pristine and well characterized hemispherical C<sub>50</sub>H<sub>10</sub> that serves as a template for a [5,5] SWCNT.(10) In a similar approach Fasel, Amsharov, and co-workers have reported the templated synthesis of [6,6] CNTs from a 90 carbon polyarene moiety prepared on a Pt(111) surface. (11) With further elaboration, either of these approaches would allow preparation of elongated [n = m] SWCNTs that could serve as thin highly conductive nanowires for numerous optoelectronic applications. Although equally synthetically challenging, an alternative approach involves the synthesis of carbon nanobelts (CNBs). In 2017, Itami and co-workers reported the synthesis of an armchair [6,6] CNB for the first time. (12,13) In 2019, the group of Miao reported the synthesis of armchair [12,12] and chiral [18,12] CNBs.(14) More recently, the Itami group has reported a zigzag [18,0] CNB.(15)

#### **Results and Discussion**

## [5,5] Fullertube Series

Recently, Stevenson and co-workers reported a new strategy for the chemical isolation of a tubular fullerene series. These represent members of a [5,5] fullertube family with half- $C_{60}$  end-caps and belts of 10 carbon atoms as illustrated for fullertubes,  $D_{5h}$ - $C_{90}$  and  $D_{5d}$ - $C_{100}$  in Figure 1.(16)

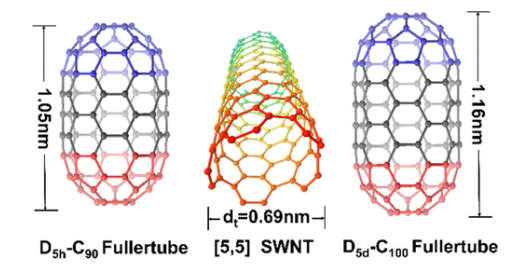


Figure 1. [5,5] SWNT,  $D_{5h}(1)$ - $C_{90}$  and  $D_{5d}(1)$ - $C_{100}$  Fullertubes:  $D_{5h}$  and  $D_{5d}$  fullerenes, but with end-caps removed, they are single-walled carbon nanotubes (SWNTs).

These tubular carbon allotropes can be selectively separated. (16) Insertion of an odd number of five-hexagon torus rings ( $D_{5h}$ - $C_{90}$  and  $D_{5h}$ - $C_{100}$ ) requires rotation of the upper cap by  $\pi/10.(17)$  This symmetry difference is readily observable in the DFT surface electrostatic maps and is especially prominent in the middle of the  $D_{5d}$  versus  $D_{5h}$  examples. All molecules described below were fully optimized utilizing the DFT B3LYP/6-31G\* level as implemented in Gaussian09 with experimental and physical characterization details provided in the  $\underline{SI}$ . The Fowler and Manolopoulos spiral program shows the subtle alteration in the spiral assembly in the Schlegel projections of  $D_{5h}(1)$ - $C_{90}$  and  $D_{5d}(1)$ - $D_{100}$  (Figure 2).(1) Spiral stripes show the same (blue) and difference (red) parts of the spiral assembly. As illustrated in Figure 3a, an amino propanol procedure permits a sample enriched in  $D_{90}$  and  $D_{100}$  fullertubes (see  $D_{100}$ ). Aliquots were removed from the reaction mixture at 30 min and 5 h (Figure 3b). HPLC analysis (PYE column, SES Research) shows a reduction of spheroidal fullerenes ( $D_{100}$ ) and an increase in the percent abundance of  $D_{100}$ 0 and  $D_{100}$ 1 fullertubes. Fractions corresponding to the  $D_{100}$ 1- $D_{100}$ 2 peak (11 min) and  $D_{100}$ 3 (19- $D_{100}$ 3 min) were collected. These data indicate that high purity samples (99.5+%) for both  $D_{100}$ 4.1- $D_{100}$ 6 and  $D_{100}$ 6 can be readily obtained.

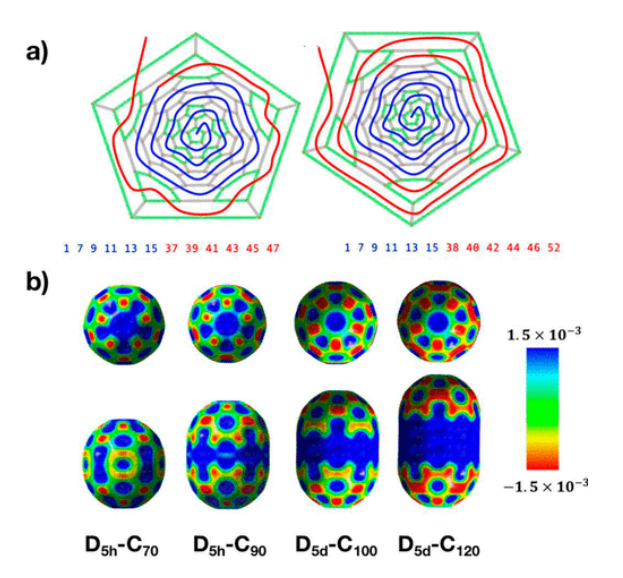


Figure 2. [5,5] Single-walled nanotube series. Schlegel projections of spiral program for (a) left,  $D_{5h}(1)$ - $C_{90}$ ; right,  $D_{5d}(1)$ - $C_{100}$  and (b) DFT electrostatic potential maps for  $D_{5h}(1)$ - $C_{70}$ ,  $D_{5h}(1)$ - $C_{90}$ ,  $D_{5d}(1)$ - $C_{100}$ , and  $D_{5d}(1)$ - $C_{120}$  (not isolated), (0.001 ebohr<sup>-3</sup>).

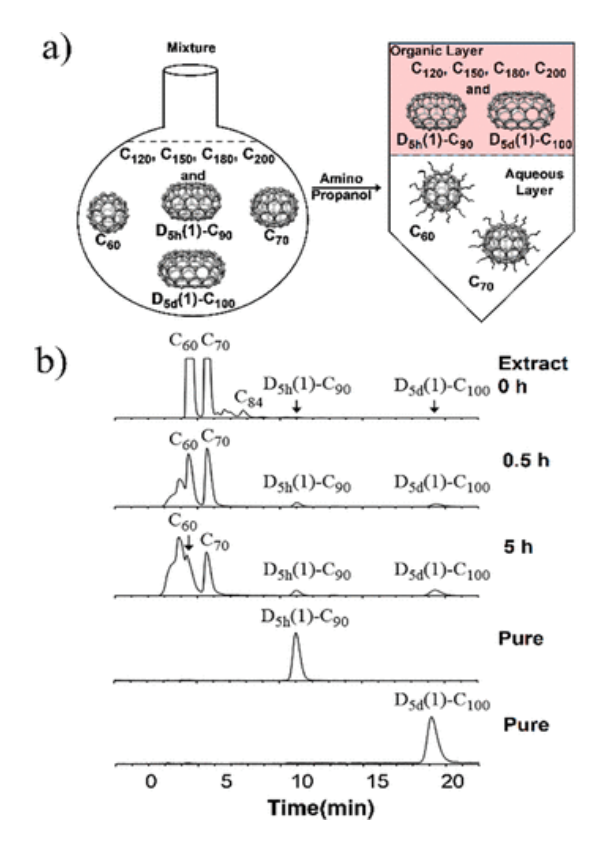


Figure 3. (a) Selective amino propanol chemical reaction to isolate the  $C_{90}$  to  $C_{100}$  fullertube series. (b) HPLC traces of the original soot extract and the HPLC trace of the extract after the selective aminopropanol chemical reaction for 0.5 h, 5 h, with HPLC collected (after 48 h) and purified  $D_{5h}(1)$ - $C_{90}$  and  $D_{5d}(1)$ - $C_{100}$  fullertubes.

In several previous studies, the HOMO–LUMO gap has been employed to predict the stability and relative abundance of fullerenes and metallofullerenes. (18,19) The DFT predicted HOMO–LUMO gaps for the  $D_{5h}$  and  $D_{5d}$  series  $C_{60}$  to  $C_{120}$  are shown in Figure 4. In contrast, smaller HOMO–LUMO gaps for  $D_{5d}$ - $C_{80}$  (1.04 eV) and  $D_{5h}$ - $C_{110}$  (0.74 eV) are consistent with their corresponding absence in the mass spectrum and chromatographic trace (Figure 3) even though they are members of this 5-fold  $C_{70}$ - $C_{120}$  series (see SI). Shinohara and co-workers previously isolated the lower abundance  $D_{5d}$ (1)- $C_{80}$  isomer (2 mg) and also  $D_2$ (2)- $C_{80}$  (5 mg) in quantities that are consistent with the low HOMO–LUMO gaps. (20) In contrast, the prominent members of the series  $D_{5h}$ - $C_{70}$ ,  $D_{5h}$ - $C_{90}$ , and  $D_{5d}$ - $C_{100}$  have HOMO–LUMO gaps above 1.0 eV. It is clear that the new chemical reaction protocol separates from a myriad of possible isomers only fullertube isomers of high symmetry.

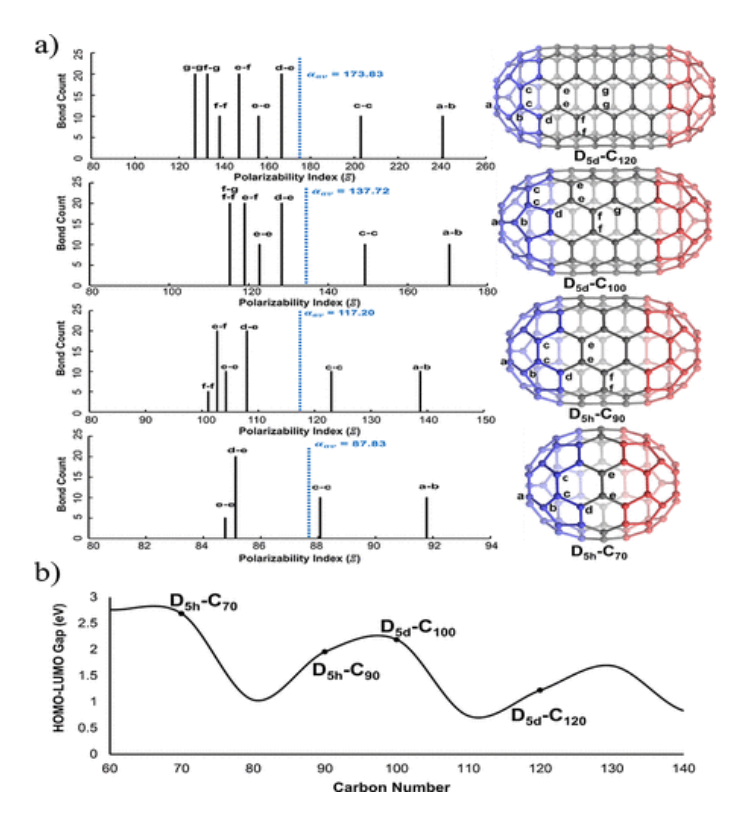


Figure 4. (a) Bond polarizability indices ( $\Xi$ ) relative to molecular polarizability (dotted blue line),  $D_{5h}$ - $C_{70}$ ,  $D_{5h}$ - $C_{90}$ ,  $D_{5d}$ - $C_{100}$ , and  $D_{5d}$ - $C_{120}$ . (b)  $D_{5d}$  and  $D_{5h}$  Fullerene DFT HOMO–LUMO Gaps. From left to right:  $D_{5h}$ - $C_{70}$ ,  $D_{5h}$ - $C_{90}$ ,  $D_{5d}$ - $C_{100}$ , and  $D_{5d}$ - $C_{120}$ . Solid line drawn as a guide to the eye.

### [5,5] Fullertube Depressed Chemical Reactivity

Of particular relevance to this chemical isolation protocol is the lower chemical reactivity of pristine tubular,  $D_{5h}(1)$ - $C_{90}$  and  $D_{5d}(1)$ - $C_{100}$  toward amination with amino propanol. In earlier reported DFT studies for the amination of [5,5] and [10,0] end-cap nanotube carbons with methylamine, both 6,6 bonds pyracylene and 6,5 pentagon carbons exhibit exothermic reaction energies in [5,5] and [10,0] nanotubes. (21) It was also established that methylamine reactivity is not significant at pentagon ring bonds. Later studies clearly show that the monoaddition of methylamine occurs specifically at 6,6 C–C junction (a-b bond, Figure 4) of the pyracylene unit in  $C_{60}$ , and the [5,5] end-caps of  $C_{120}$  are significantly more energetically favorable in comparison with the addition to other 6,6 and 5,6 C–C junctions. (22) Sabirov has shown that a polarization model is useful for understanding the modes of ozone and diazomethane addition to higher fullerenes,  $D_{5h}$ - $C_{70}$ ,  $D_2$ - $C_{76}$ , and  $C_{2v}$ - $C_{78}$ , which have inequivalent double bonds. (23,24) This polarizability model predicts the same 6,6 C–C junction as found for the earlier amination studies as illustrated in Figure 4.

The Sabirov approach considers the fullerene molecule as a polarizable ellipsoid in a polar coordinate system (origin is at the center of mass of the molecule) and assigns each reaction center a point (different carbon atom) belonging to the polarizability ellipsoid and characterized by the polarizability  $\xi$  which is in

the direction of the reaction center. The polarizability index  $\Xi$  was determined as the average between

$$\xi = \left(\frac{\sin^2\!\psi\cos^2\!\phi}{\alpha_{xx}^2} + \frac{\sin^2\!\psi\sin^2\!\phi}{\alpha_{yy}^2} + \frac{\cos^2\!\psi}{\alpha_{zz}^2}\right)^{-0.5}$$
 two adjacent sites (bond). 
$$(1)^{\Xi} = 0.5(\xi_1 + \xi_2)(2)$$

As illustrated in Figure 4, a specific 6,6 C–C junction (a-b) exhibits a much larger polarizability index than any other carbon bond for the end-caps of  $D_{5h}(1)$ - $C_{70}$ ,  $D_{5h}(1)$ - $C_{90}$ , and  $D_{5d}(1)$ - $C_{100}$ . Although a second 5,6 C–C bond (b-c) slightly exceeds the Sabirov criteria for low reactivity ( $\Xi < \alpha_{av}$ ), the earlier DFT amination studies and the significantly greater reactivity predicted by the polarizability index for the a-b bond suggest a greater reactivity for the a-b bond. The polarizability index predicts a high chemical reactivity for only one type of 6,6 bond (10 bonds total) in the end-cap of these [5,5] tubular fullerenes. The trend for the series  $D_{5h}(1)$ - $C_{70}$ ,  $D_{5h}(1)$ - $C_{90}$ , and  $D_{5d}(1)$ - $C_{100}$  is an increasing number of nonreactive bonds ( $\Xi < \alpha_{av}$ ) relative to the more reactive 6,6 bonds, and the reaction rate should decrease with increasing tube length. In addition, lower symmetry ellipsoidal and spherical isomers for  $C_{90}$  and  $C_{100}$  should exhibit a higher reactivity toward amination.

## $D_{5h}(1)$ - $C_{90}$ and $D_{5d}(1)$ - $C_{100}$ Physical Characterization

### UV-vis

The UV–vis experimental spectra were obtained for isolated  $D_{5h}(1)$ - $C_{90}$  and  $D_{5d}(1)$ - $C_{100}$  fullertube species and compared to published spectra (see SI).(16) The  $D_{5h}(1)$ - $C_{90}$  UV–vis spectrum was also previously published by Yang et al.(4) In that work, three  $C_{90}$  isomers were characterized by UV–vis with corresponding X-ray crystal structures.(4) We have compared DFT calculations that predict the major features of the UV–vis  $D_{5h}(1)$ - $C_{90}$  and  $D_{5d}(1)$ - $C_{100}$  (see SI). When dissolved in carbon disulfide, the  $D_{5d}(1)$ - $C_{100}$  has peak maxima at 410 nm, 661 nm, and a large peak at 574 nm that dominates the predicted UV–vis spectrum. It should be noted that  $C_{60}$  also has peaks at 540, 560, and 600 nm consistent with the complementary purplish color of  $I_h$ - $C_{60}$  and  $D_{5d}(1)$ - $C_{100}$  (see SI).(16,25)

## <sup>13</sup>C NMR

The X-ray single crystal structure has been obtained for  $D_{5d}(1)$ - $C_{100}$ , but the  $^{13}C$  NMR spectra for this sample have not been reported. (12) The  $^{13}C$  NMR chemical shift is an important parameter to define the diameter of semiconductor and metallic SWNTs. (26) The  $^{13}C$  NMR spectra for the isolated  $C_{90}$  and  $C_{100}$  fullerenes are shown in Figure 5a and consists of only 6 observed lines. The  $C_{90}$  isomer has 4 pyracylene 6,6,5 carbon sites that range in chemical shifts from 153.6 to 133.7 ppm for the end-capped carbons to the belt carbons. The poor S/N ratio limits the predicted intensity ratios with the aberrant intensity peak at 153.6 ppm, but the other 6,6,5 peaks are in qualitative agreement. The 6,6,6 junction belt carbons exhibit  $^{13}C$  NMR chemical shifts of 132.2 and 128.5 ppm with the expected intensities of 10 and 20, respectively. In addition, the DFT computational results for  $D_{5d}(1)$ - $C_{90}$  are in agreement with the experimental data and all predicted values are within  $\sim$ 2.5 ppm.

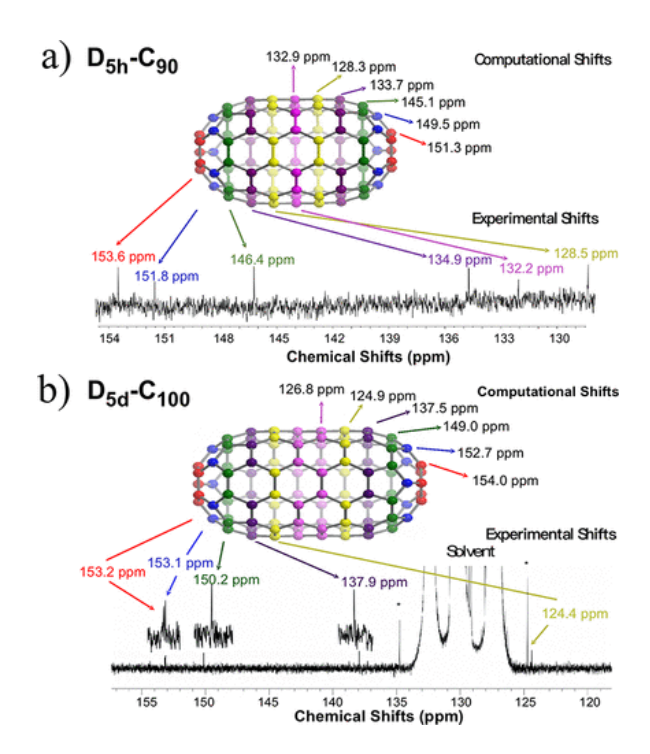


Figure 5. DFT computational NMR shifts vs experimental chemical shifts for (a)  $D_{5h}(1)$ - $C_{90}^{13}$ C 150 MHz (14.1 T) NMR spectrum, in carbon disulfide,  $Cr(acac)_3$  added, and (b)  $D_{5d}(1)$ - $C_{100}$ ,  $^{13}$ C 200 MHz (18.8 T) NMR spectrum in o- $d_4$ -dichlorobenzene,  $Cr(acac)_3$  added, and 77 h of scan time.

Consistent with the experimental <sup>13</sup>C NMR spectrum, the IPR allowed C<sub>100</sub> fullerenes have only 3 high symmetry IPR isomers with fewer than 10 spectral lines,  $D_{5d}(1)-C_{100}$  (2 × 10, 4 × 20), T(321)-C<sub>100</sub>, (1 × 4, 8 × 12), and  $D_5(450)$ - $C_{100}$  (10 × 10). The isolated  $C_{100}$  sample was limited by poor solubility in most solvents, but a  $^{13}$ C 200 MHz (18.8 T) NMR spectrum was obtained in o- $d_4$ -dichlorobenzene and required 77 h of scan time (Figure 5b). The C100 isomer has 4 pyracylene 6,6,5 carbon sites that range in chemical shifts from 153.2 to 138.0 ppm for the end-capped carbons to the belt carbons with correct intensity ratios of 10, 10, 20, 20, and 20, respectively. The DFT 6,6,6 junction belt carbons have predicted <sup>13</sup>C NMR chemical shifts of 124.9 and 126.8 ppm, but only a peak at 124.4 was observable in agreement with the most shielded carbon. The "missing"  $^{13}$ C NMR signal for the  $D_{5d}(1)$ - $C_{100}$  sample is most likely concealed under the intense o-d<sub>4</sub>-dichlorobenzene solvent lines. It should be noted that the <sup>13</sup>C NMR experimental and computational data are consistent for the D<sub>5d</sub>(1)-C<sub>100</sub> isomer with 5 out of the predicted 6 <sup>13</sup>C NMR experimental peaks within 0.5-1.2 ppm of the DFT computational values, and the 6,6,5 carbon sites have the predicted intensity ratios (10, 10, 20, and 20) for this isomer. The first belt carbon attached to the endcap for  $D_{5h}(1)$ - $C_{90}$  has a shift of 128.5 ppm which is 4 ppm higher than the same carbon site for  $D_{5d}(1)$ -C<sub>100</sub> (124.4 ppm). This is in excellent agreement with the results by Engtrakul and co-workers who observed <sup>13</sup>C chemical shifts for metallic SWCNTs shifted to lower frequency by 3-4 ppm relative to semiconducting SWCNTs with similar diameters (0.77 and 0.82 nm).(26)

### **XPS**

The XPS spectra for the  $D_{5h}(1)$ - $C_{90}$  and  $D_{5d}(1)$ - $C_{100}$  samples are shown (<u>Figure 6</u>a,b). The carbon 1s XPS spectra for the tubular fullertubes  $D_{5h}(1)$ - $C_{90}$  and  $D_{5d}(1)$ - $C_{100}$  are positioned at binding energies of  $\sim$ 285.0

eV and fwhm of 1.15 and 1.00 eV, respectively. Of particular interest, there is no evidence of asymmetry in the C 1s peaks for either  $D_{5h}(1)$ - $C_{90}$  and  $D_{5d}(1)$ - $C_{100}$ . The C 1s XPS spectrum reported for long metallic SWNTs with larger diameters ( $d_t \sim 1.5$  nm) are shifted to lower energy in the C 1s band and a smaller fwhm (284.4 and 0.77 eV). Their study has shown that the carbon 1s peak is significantly shifted for silver chloride filled metallic nanotubes and broadening is usually observed when charge is introduced into a SWCNT.(27) In addition, although the XPS spectrum for the  $D_{5h}(1)$ - $C_{90}$  sample exhibits evidence for a trace amount of oxygen, (small O 1s peak  $\sim 530$  eV), there is no evidence of any significant C–O bond formation which would lead to a side peak for C 1s peak at  $\sim 286$  eV (Figure 6b). The influence of elevated temperatures (300 °C) were also explored for the  $D_{5d}(1)$ - $C_{100}$  sample (Figure 6c), but the C 1s peak remains symmetric with a binding energy and fwhm of 285.1 and 1.00 eV. The elevated temperature (300 °C) XPS spectrum for the valence band for the  $D_{5d}(1)$ - $C_{100}$  sample is shown in the SI.

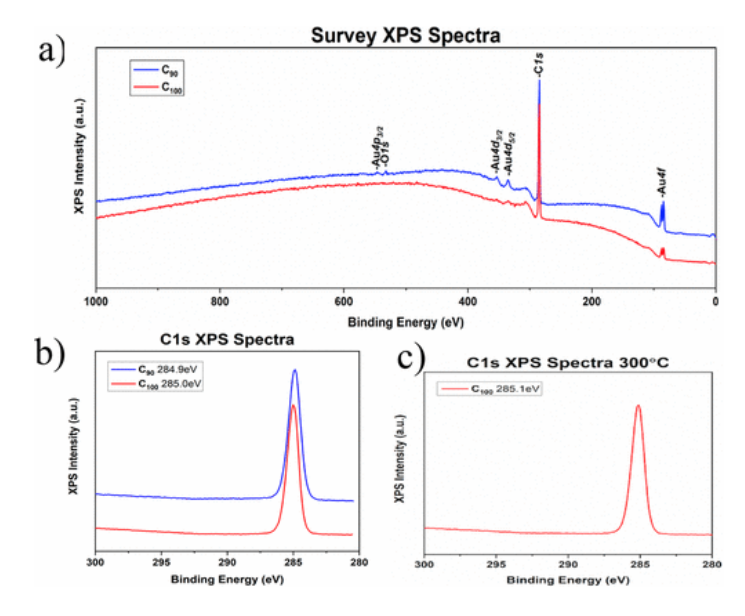


Figure 6. (a) Survey XPS spectra for  $D_{5h}(1)$ - $C_{90}$  and  $D_{5d}(1)$ - $C_{100}$  on Au surface. (b) Expanded C 1s XPS Spectra of  $D_{5h}(1)$ - $C_{90}$  and  $D_{5d}(1)$ - $C_{100}$ . (c) 300 °C C 1s XPS of  $D_{5d}(1)$ - $C_{100}$ .

# **EPR**

The X-band EPR data (0.33T) was also obtained for solid  $C_{60}$ ,  $D_{5h}(1)$ - $C_{70}$ ,  $D_{5h}(1)$ - $C_{90}$ , and  $D_{5d}(1)$ - $C_{100}$  (SI). An asymmetric peak (nondegassed) was obtained for all samples with nearly equivalent g factors of 2.000  $\pm$  0.006. These results are consistent with the report by Reed and co-workers of the presence of a fullerene epoxide, (e.g.,  $C_{60}O$ ) in many fullerene samples exposed to  $O_2$  with a g factor of 2.0026. (28) However, no significant difference in the EPR spectra was observed for these samples with no apparent evidence of itinerant electrons associated with a higher g factor (g = 2.07). (29)

# Raman

As previously noted, the electronic properties of SWCNTs critically depend on their structure, which is characterized by the chiral index (n,m) that denotes a vectorial orientation of the rolled-up hexagonal carbon lattice. On the basis of previous studies, SWNTs with n = m are predicted to be metallic and exhibit properties characteristic of highly conductive thin nanowires. (8,9) However, for the case of

[5,5] fullertubes, additional factors are important when assessing the electronic properties, such as the tube length, closed end-caps, and small diameter ( $d_t$  = 0.69 nm).(30-34) The two Raman features most commonly employed to characterize SWNTs are the G-band at ~1580–1600 cm<sup>-1</sup>, a vibrational mode common to all sp<sup>2</sup> carbons and the radial breathing mode (RBM) which is a characteristic mode exclusive for all SWCNTs. The Raman spectral data for  $D_{sh}(1)$ - $C_{90}$  and  $D_{sd}(1)$ - $D_{100}$  and expansions of the G band and RBM are shown in Figure 7a,b. The RBM features correspond to the coherent vibration of carbon atoms in the radial direction, and characterized as a "breathing" mode. For the RBM region, there are several peaks in this region for these [5,5] fullertubes, therein confirming a classification as SWNTs. Although a RBM mode can usually predict the nanotube diameter for isolated SWNTs, this simple linear relationship does not hold for small nanotubes because of significant lattice distortions of nanotubes with widths,  $d_t < 1$  nm.(31) Kurti and co-workers considered this issue for small diameter tubes with  $\omega_{DFT} = 234/d_t$ , and they predicted values ranging from 337 to 339 cm<sup>-1</sup> for [5,5] nanotubes,  $d_t = 0.69$  cm<sup>-1</sup>.(33) To account for van der Waals interaction(s) with the environment, Dresselhaus and co-workers presented a revised RBM equation for predicting the diameter of nanotubes(34) $\omega_{DFT} = 227/d_t \sqrt{1 + C_c} d_t^2$ ,  $C_c = 0.05 - 0.07$ (3)

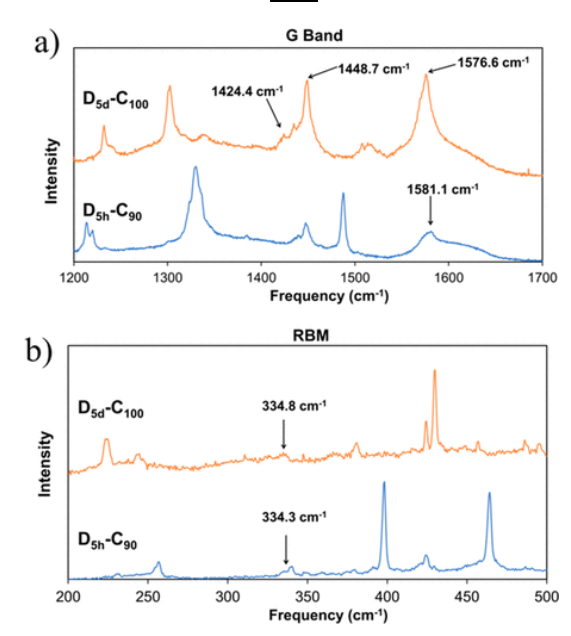


Figure 7. Raman spectral data for  $D_{5h}(1)$ - $C_{90}$  and  $D_{5d}(1)$ - $C_{100}$  and expansions of the (a) G band and (b) RBM band.

For [5,5] fullertubes ( $d_t = 0.69$  nm), this calculation leads to a predicted value of 333.6 cm.<sup>-1</sup> For the  $D_{5h}(1)$ - $C_{90}$  and  $D_{5d}(1)$ - $C_{100}$  samples, there are small peaks, 334.3 and 334.8 cm<sup>-1</sup>, respectively, which are in excellent agreement with this prediction (<u>Figure 7</u>). As expected, it is important to note that for a heated sample of  $D_{5d}(1)$ - $C_{100}$  (300 °C), the 334.8 cm<sup>-1</sup> mode is broadened and attenuated with only 3 prominent peaks remaining in the RBM region at 551, 427, and 223.4 cm<sup>-1</sup> (<u>SI</u>). It is well recognized that a Breit-Wigner-Fano (BWF) line shape is needed to fit the tangential G band for metallic carbon nanotubes with a higher frequency Lorentzian line-shape factor ( $\sim$ 1600 cm<sup>-1</sup>) and lower frequency BWFT components (1577 and 1545 cm<sup>-1</sup>).(<u>30)</u> The  $D_{5h}(1)$ - $C_{90}$  and  $D_{5d}(1)$ - $C_{100}$  samples exhibit maximum peaks at 1581.1 and 1576.6 cm<sup>-1</sup>, respectively. In addition, the  $D_{5d}(1)$ - $C_{100}$  sample exhibits a weak sideband peak at  $\sim$ 1548 cm<sup>-1</sup>

¹ consistent with metallic character for the  $D_{5d}(1)$ - $C_{100}$  sample (see  $\underline{SI}$ ). In addition, the G band consists of two major bands ( $G^+$  and  $G^-$ ) with the former dependent on vibration modes between two dissimilar carbon atoms in the SWNT and is independent of the SWNT diameter. $\underline{(31)}$  The  $G^+$  mode approaches the value for graphite of 1591 cm<sup>-1</sup> for large diameter SWNTs, whereas the  $G^-$  mode is dependent on the diameter and whether the SWNT is metallic or a semiconductor. This has been expressed as  $G^-$  = 1591 cm<sup>-1</sup>-A/dt², where ( $A_{G^-}$ )<sup>S</sup> = 47.7 and ( $A_{G^-}$ )<sup>M</sup> = 79.5 cm<sup>-1</sup>/(nm)² for semiconducting and metallic SWNTs, respectively (see Figure 8). The Raman G modes are summarized for the [5,5] fullertube series of  $C_{70}(D_{5h})$ ,  $D_{5h}(1)$ - $C_{90}$ , and  $D_{5d}(1)$ - $C_{100}$  with 1, 3, and 4-hexagon torus rings between the upper and lower halve- $C_{60}$  caps. Although  $D_{5h}(1)$ - $C_{90}$  has  $G^-$  bands consistent with semiconductors, the longer  $D_{5d}(1)$ - $C_{100}$  fullertube is consistent with metallic properties with two prominent 1449.2 and 1424.4 cm<sup>-1</sup> modes which are reasonably close to the predicted metallic value of 1426.4 cm<sup>-1</sup>.

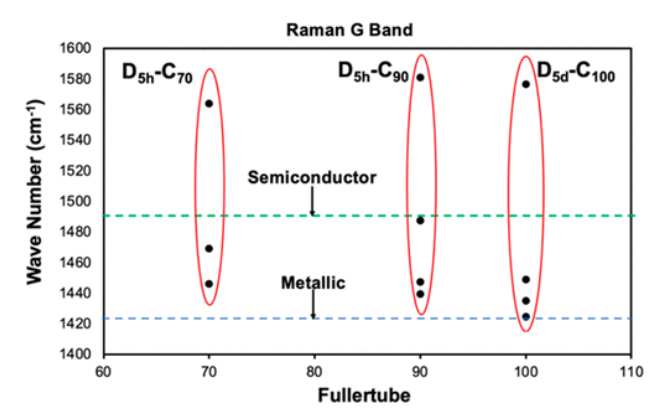


Figure 8. Raman G band for  $C_{70}(D_{5h})$ ,  $C_{90}(D_{5h})$ , and  $C_{100}(D_{5d})$ : Raman data for  $C_{70}(D_{5h})$  are obtained from data reported by Kappes and co-workers. (35) Dotted lines are predicted semiconductor and metallic lines,  $G^- = 1591 \text{ cm}^{-1}$ -A/dt², dt = 0.69 nm;  $(A_{G^-})^S = 47.7$  and  $(A_{G^-})^M = 79.5 \text{ cm}^{-1}$ /(nm)², respectively.

Since [n = m] single-walled carbon nanotubes (SWNT) are usually not end-capped and normally exhibit variable nanotube diameters (d<sub>t</sub>) with large aspect ratios, it is relevant to consider whether pristine [5,5] end-capped fullertubes with small aspect ratios veritably exhibit metallic character. Our experimental  $^{13}$ C NMR and Raman results support the argument of metallic character for  $D_{5d}(1)$ - $C_{100}$ , but the argument is tenuous for  $D_{5h}(1)$ - $C_{90}$ . As previously indicated, the seminal study by Mintmire and colleagues consists of a DFT model of a tubule constructed from 10 rings with  $D_{5h}$  symmetry.(8) A further description of their [5,5] nanotube model leads to a Fermi crossing of irreducible representations (a<sub>1</sub> and a<sub>2</sub>) at k =  $2\pi/3$  in the Brillouin zone. This Fermi crossing represents a breaking of symmetry from a single ten-carbon ring to three ten-carbon ring units. Since  $D_{5h}(1)$ - $C_{90}$  and  $D_{5d}(1)$ - $C_{100}$  have three and four ten-carbon tubular ring units, it is reasonable conjecture that metallic character starts with  $D_{5d}(1)$ - $C_{100}$ . This also leads to the prediction that other members of the [5,5] fullertube family with higher aspect ratios will also be metallic.

## **Conclusions**

The results of the current study demonstrate isolation and physical characterization of pristine  $D_{5h}(1)$ - $C_{90}$  and  $D_{5d}(1)$ - $C_{100}$  by selective chemical regio-reactivity and methodology for isolating additional pristine members of the [5,5] fullertube family. From the chemical reactivity protocol and mass spectral data, it is clearly possible to isolate pristine tubular fullerenes larger than  $C_{100}$ . Since single-walled carbon nanotube

(SWNT) samples usually consist of mixtures with variations based on tube diameter, length, and chirality, the availability of pristine [5,5] end-capped fullertubes from  $C_{100}$ - $C_{180}$  will provide unique pristine samples for a myriad of potential electronic applications. Our <sup>13</sup>C NMR and Raman results suggest that pristine  $D_{5h}(1)$ - $C_{90}$  more likely exhibits semiconducting electronic properties, but  $D_{5d}(1)$ - $C_{100}$  is predicted to be metallic. As previously reported, semiconducting SWNTs with belt carbons adjacent to end-caps exhibit <sup>13</sup>C chemical shifts of 125–130 ppm, whereas metallic SWNTs exhibit shifts 3–4 ppm lower. (26) In addition, the Raman results for the BWF line shape and  $G^-$ band are consistent with semiconducting and metallic properties for  $D_{5h}(1)$ - $C_{90}$  and  $D_{5d}(1)$ - $C_{100}$ , respectively. As previously indicated, the [5,5] fullertubes are short armchair SWNTs that are expected to exhibit metallic behavior different from ordinary metals and should result in exceptional ballistic transport properties. Finally, the chemical separation/mass spectral analysis protocol for the [5,5] nanotube-fullerene family could be an important fingerprint for future studies of fullerene or nanotube samples from other terrestrial and extraterrestrial sources. (36) To illustrate, carbon nanotubes with diameters close to [5,5] fullertubes ( $d_t = 0.6$  nm) have been reported in pottery shards found in India dated to ~2600 years old. (37)

## **Supporting Information**

The Supporting Information is available free of charge at <a href="https://pubs.acs.org/doi/10.1021/jacs.0c11357">https://pubs.acs.org/doi/10.1021/jacs.0c11357</a>.

Description of the fullertube isolation procedure, colored images of solutions of fullertubes, DFT calculated UV-vis vs experimental data, EPR X-band and <sup>13</sup>C NMR data for fullertubes, Raman SERS preparation, expanded spectra, and elevated temperature data for the fullertubes. DFT computational details and x, y, and z coordinates for the <sup>13</sup>C NMR spectra (<u>PDF</u>)

## **Author Information**

# **Corresponding Authors**

Steven Stevenson - Department of Chemistry, Purdue University Fort Wayne, Fort Wayne, Indiana 46805, United States; Orcidhttp://orcid.org/0000-0003-3576-4062; Email: stevenss@pfw.edu

Harry C. Dorn - Department of Chemistry, Virginia Tech, Blacksburg, Virginia 24061, United States; Orcidhttp://orcid.org/0000-0002-3150-5314; Email: <a href="mailto:hdorn@vt.edu">hdorn@vt.edu</a>

# **Authors**

Xiaoyang Liu - Department of Chemistry, Virginia Tech, Blacksburg, Virginia 24061, United States

D. Mathew Sublett - Department of Geosciences, Virginia Tech, Blacksburg Virginia 24061, United States

Ryan M. Koenig - Department of Chemistry, Purdue University Fort Wayne, Fort Wayne, Indiana 46805, United States

Tiffany L. Seeler - Department of Chemistry, Purdue University Fort Wayne, Fort Wayne, Indiana 46805, United States

Katelyn R. Tepper - Department of Chemistry, Purdue University Fort Wayne, Fort Wayne, Indiana 46805, United States

Hannah M. Franklin - Department of Chemistry, Purdue University Fort Wayne, Fort Wayne, Indiana 46805, United States

Xiaoling Wang - National High Magnetic Field Laboratory, Tallahassee, Florida 32310, United States

Rong Huang - Department of Chemistry, Virginia Tech, Blacksburg, Virginia 24061, United States

Xu Feng - Department of Chemistry, Virginia Tech, Blacksburg, Virginia 24061, United States; Orcidhttp://orcid.org/0000-0003-1945-1605

Kevin Cover - Department of Chemistry, Virginia Tech, Blacksburg, Virginia 24061, United States

Diego Troya - Department of Chemistry, Virginia Tech, Blacksburg, Virginia 24061, United States; Orcidhttp://orcid.org/0000-0003-4971-4998

Narasimhamurthy Shanaiah - Department of Chemistry, Virginia Tech, Blacksburg, Virginia 24061, United States

Robert J. Bodnar - Department of Geosciences, Virginia Tech, Blacksburg Virginia 24061, United States

**Author Contributions** 

All authors significantly contributed to this research.

#### Notes

The authors declare no competing financial interest.

# **Acknowledgments**

We thank the Surface Analysis Laboratory at Virginia Tech for the XPS analysis supported by the National Science Foundation under Grant No. CHE-1531834. S.S. thanks the National Science Foundation for RUI Grant CHE-1856461 for financial support. Advanced Research Computing at Virginia Tech is gratefully acknowledged for the computational resources used in this work.

### References

- 1. Fowler, P. W.; Manolopoulos, D. E. An Atlas of Fullerenes; Clarendon Press: Oxford, 1995, 1–289.
- 2. Xu, J.; Wang, Z.; Shi, Z.; Gu, Z. Synthesis, Isolation and Spectroscopic Characterization of Yb-Containing High Metallofullerenes. Chem. Phys. Lett. 2005, 409 (4), 192–196, DOI: 10.1016/j.cplett.2005.05.034
- 3. Yang, H.; Mercado, B. Q.; Jin, H.; Wang, Z.; Jiang, A.; Liu, Z.; Beavers, C. M.; Olmstead, M. M.; Balch, A. L. Fullerenes without Symmetry: Crystallographic Characterization of C1(30)-C90 and C1(32)-C90. Chem. Commun. 2011, 47 (7), 2068–2070, DOI: 10.1039/C0CC03017A
- 4. Yang, H.; Beavers, C. M.; Wang, Z.; Jiang, A.; Liu, Z.; Jin, H.; Mercado, B. Q.; Olmstead, M. M.; Balch, A. L. Isolation of a Small Carbon Nanotube: The Surprising Appearance of D5h(1)-C90. Angew. Chem., Int. Ed. 2010, 49 (5), 886–890, DOI: 10.1002/anie.200906023

- 5. Bowles, F. L.; Mercado, B. Q.; Ghiassi, K. B.; Chen, S. Y.; Olmstead, M. M.; Yang, H.; Liu, Z.; Balch, A. L. Ordered Structures from Crystalline Carbon Disulfide Solvates of the Nano-Tubular Fullerenes D5h(1)-C90 and D5h-C70. Cryst. Growth Des. 2013, 13 (10), 4591–4598, DOI: 10.1021/cg401138g
- 6. Iijima, S.; Ichihashi, T. Single-shell carbon nanotubes of 1-nm diameter. Nature 1993, 363, 603–605, DOI: 10.1038/363603a0
- 7. Bethune, D. S.; Kiang, C. H.; DeVries, M. S.; Gorman, G.; Savoy, R.; Vazquez, J.; Beyers, R. Cobalt-Catalyzed Growth of Carbon Nanotubes with Single-Atomic-Layer Walls. Nature 1993, 363, 605–607, DOI: 10.1038/363605a0
- 8. Mintmire, J. W.; Dunlap, B. I.; White, C. T. Are Fullerene Tubules Metallic?. Phys. Rev. Lett. 1992, 68, 631–634, DOI: 10.1103/PhysRevLett.68.631
- 9. White, C. T.; Todorov, T. N. Carbon Nanotubes as Ballistic Conductors. Nature 1998, 393, 240–242, DOI: 10.1038/30420
- 10. Scott, L. T.; Jackson, E. A.; Zhang, Q.; Steinberg, B. D.; Bancu, M.; Li, B. A Short, Rigid, Structurally Pure Carbon Nanotube by Stepwise Chemical Synthesis. J. Am. Chem. Soc. 2012, 134, 107–110, DOI: 10.1021/ja209461g
- 11. Sanchez-Valencia, J. R.; Dienel, T.; Groning, O.; Shorubalko, I.; Mueller, A.; Jansen, M.; Amsharov, K.; Ruffieux, P.; Fasel, R. Nature 2014, 512, 61–64, DOI: 10.1038/nature13607
- 12. Povie, G.; Segawa, Y.; Nishihara, T.; Miyauchi, Y.; Itami, K. Synthesis of a Carbon Nanobelt. Science 2017, 356, 172–175, DOI: 10.1126/science.aam8158
- 13. Povie, G.; Segawa, Y.; Nishihara, T.; Miyauchi, Y.; Itami, K. Synthesis and Size-Dependent Properties of [12], [16], and [24] Carbon Nanobelts. J. Am. Chem. Soc. 2018, 140, 10054–10059, DOI: 10.1021/jacs.8b06842
- 14. Cheung, K. Y.; Gui, S.; Liu, Z.; Chi, L.; Miao, Q. Synthesis of Armchair and Chiral Carbon Nanobelts. Chem. 2019, 5, 838–847, DOI: 10.1016/j.chempr.2019.01.004
- 15. Cheung, K. Y.; Watanabe, K.; Segawa, Y.; Itami, K. Synthesis of a Zig-Zag Carbon Nanobelt. Nat. Chem. 2021, 13, 255–259, DOI: 10.1038/s41557-020-00627-5
- Koenig, R. M.; Tian, H. R.; Seeler, T. L.; Tepper, K. R.; Franklin, H. M.; Chen, Z. C.; Xie, S. Y.; Stevenson, S. Fullertubes: Cylindrical Carbon with Half-Fullerene End-Caps and Tubular Graphene Belts, Their Chemical Enrichment, Crystallography of Pristine C90-D5h(1) and C100-D5d(1) Fullertubes, and Isolation of C108, C120, C132 and C156 Cages of Unknown Structures. J. Am. Chem. Soc. 2020, 142 (36), 15614–15623, DOI: 10.1021/jacs.0c08529
- 17. Bodner, M.; Patera, J.; Szajewska, M. C70, C80, C90 and Carbon Nanotubes by Breaking of the Icosahedral Symmetry of C60. Acta Crystallographica Section A: Foundations of Crystallography 2013, 69 (6), 583–591
- 18. Hirsch, A.; Brettreich, M. Fullerenes: Chemistry and Reactions; Wiley-VCH Verlag GmbH & Co. KGaA John Wiley & Sons: Weinheim, 2005, 1–423.

- 19. Yoshida, M.; Aihara, J. Validity of the Weighted HOMO-LUMO Energy Separation as an Index of Kinetic Stability for Fullerenes up to 120 Carbon Atoms. Phys. Chem. Chem. Phys. 1999, 1, 227–230, DOI: 10.1039/a807917j
- 20. Wang, C. R.; Sugai, T.; Kai, T.; Tomiyama, T.; Shinohara, H. Production and Isolation of an Ellipsoidal C80 Fullerene. Chem. Commun. 2000, 557–558, DOI: 10.1039/b000387p
- 21. Basiuk, E. V.; Monroy-Peláez, M.; Puente-Lee, I.; Basiuk, V. A. Direct Solvent-Free Amination of Closed-Cap Carbon Nanotubes: A Link to Fullerene Chemistry. Nano Lett. 2004, 4 (5), 863–866, DOI: 10.1021/nl049746b
- 22. Lin, T.; Zhang, W.-D.; Huang, J.; He, C. A DFT Study of the Amination of Fullerenes and Carbon Nanotubes: Reactivity and Curvature. J. Phys. Chem. B 2005, 109 (28), 13755–13760, DOI: 10.1021/jp051022g
- 23. Sabirov, D. S.; Bulgakov, R. G.; Khursan, S. L.; Dzhemilev, U. M. A New Approach to the Estimation of the Fullerene Reactivity in 1, 3-Dipolar Addition Based on Polarizability Indices. Dokl. Phys. Chem. 2009, 425, 54–56, DOI: 10.1134/S0012501609030026
- 24. Sabirov, D. Polarizability as a Landmark Property for Fullerene Chemistry and Materials Science. RSC Adv. 2014, 4 (85), 44996–45028, DOI: 10.1039/C4RA06116K
- 25. Hare, J. P.; Kroto, H. W.; Taylor, R. Preparation and UV/Visible Spectra of Fullerenes C60 and C70. Chem. Phys. Lett. 1991, 177 (4–5), 394–398, DOI: 10.1016/0009-2614(91)85072-5
- Engtrakul, C.; Irurzun, V. M.; Gjersing, E. L.; Holt, J. M.; Larsen, B. A.; Daniel, E.; Resasco, D. E.; Jeffrey, L.; Blackburn, J. L. Unraveling the 13C NMR Chemical Shifts in Single-Walled Carbon Nanotubes: Dependence on Diameter and Electronic Structure. J. Am. Chem. Soc. 2012, 134, 4850–4856, DOI: 10.1021/ja211181q
- 27. Kharlamova, M. V.; Kramberger, C.; Domanov, O.; Mittelberger, A.; Yanagi, K.; Pichler, T.; Eder, D. Fermi level engineering of metallicity-sorted metallic single-walled carbon nanotubes by encapsulation of few-atom-thick crystals of silver chloride. J. Mater. Sci. 2018, 53, 13018–13029, DOI: 10.1007/s10853-018-2575-y
- 28. Paul, P.; Kim, K.-C.; Sun, D.; Boyd, P. D. W.; Reed, C. A. Artifacts in the Electron Paramagnetic Resonance Spectra of C60 Fullerene Ions: Inevitable C1200 Impurity. J. Am. Chem. Soc. 2002, 124, 4394–4401, DOI: 10.1021/ja011832f
- 29. Corzilius, B.; Dinse, K. P.; Hata, K.; Haluška, M.; Skákalová; Roth, S. SWNT probed by multi-frequency EPR and nonresonant microwave SWNT probed by multi-frequency EPR and nonresonant microwave absorption absorption. Phys. Status Solidi B 2008, 245 (10), 2251–2254, DOI: 10.1002/pssb.200879574
- 30. Brown, S. D. M.; Jorio, A.; Corio, P.; Dresselhaus, G.; Saito, R.; Kneipp, K. Origin of the Breit-Wigner-Fano lineshape of the tangential G-band feature of metallic carbon nanotubes. Phys. Rev. B: Condens. Matter Mater. Phys. 2001, 63, 155414—155417, DOI: 10.1103/PhysRevB.63.155414
- 31. Dresselhaus, M.S.; Dresselhaus, G.; Saito, R.; Jorio, A. Raman spectroscopy of carbon nanotubes. Phys. Rep. 2005, 409, 47–99, DOI: 10.1016/j.physrep.2004.10.006

- 32. Bachilo, M. S.; Strano, M. S.; Kittrell, C.; Hauge, R. H.; Smalley, R. E.; Weisman, R. B. Structure-Assigned Optical Spectra of Single-Walled Carbon Nanotubes. Science 2002, 298, 2361–2366, DOI: 10.1126/science.1078727 [Crossref], [PubMed], [CAS], Google ScholarOpenURL PURDUE UNIV FORT WAYNE
- 33. Kurti, J.; Zolyomi, V.; Kertesz, M.; Sun, G. The geometry and the radial breathing mode of carbon nanotubes: beyond the ideal behaviour. New J. Phys. 2003, 5, 125
- 34. Dresselhaus, M. S.; Jorio, A.; Hofmann, M.; Dresselhaus, G.; Saito, R. Perspectives on Carbon Nanotubes and Graphene Raman Spectroscopy. Nano Lett. 2010, 10, 751–758, DOI: 10.1021/nl904286r
- 35. Lebedkin, S.; Hull, W. E.; Soldatov, A.; Renker, B.; Kappes, M. R. Structure and Properties of the Fullerene Dimer C140 Produced by Pressure Treatment of C70. J. Phys. Chem. B 2000, 104, 4101–4110, DOI: 10.1021/jp994330l
- 36. Becker, L.; Poreda, R. J.; Bunch, T. E. Fullerenes: An Extraterrestrial Carbon Carrier Phase for Noble Gases. Proc. Natl. Acad. Sci. U. S. A. 2000, 97 (7), 2979–2983, DOI: 10.1073/pnas.97.7.2979
- 37. Kokarneswaren, M.; Selvaraj, P.; Ashokan, T.; Perumal, S.; Sellappan, P.; Murugan, K. D.; Ramalingam, S.; Mohan, N.; Chandrasekaren, V. Discovery of Carbon Nanotubes in Sixth Century BC Potteries from Keeladi, India. Sci. Rep. 2020, 10, 19786, DOI: 10.1038/s41598-020-76720-z